Ultrasound-targeted microbubble destruction technology delivering β-klotho to the heart enhances FGF21 sensitivity and attenuates heart remodeling post-myocardial infarction

CHAOFU YUE[1-3*], RONG LI[1*], CHUNYAN LI[4], TAOXIAN YANG[5], XIAN HUANG[1], RONG LEI[1], YONGJUN YAN[1], YUAN LIU[1], QIAOLIN LI[1], QINYONG YAN[1], DINGRONG ZUO[1], SHISHENG LIU[1] and MEI YANG[1-3]

[1]Department of Intensive Care Unit, Qujing First People's Hospital, Qujing, Yunnan 655099, P.R. China; [2]Kunming Medical University, Yunnan University Medical Bioengineering Center, Kunming, Yunnan 650500, P.R. China; [3]Kunming Institute of Zoology, Chinese Academy of Sciences, Kunming, Yunnan 650500, P.R. China; [4]Department of Endocrinology and Metabolism, Qujing First People's Hospital, Qujing, Yunnan 655099, P.R. China; [5]Nursing Department, Qujing First People's Hospital, Qujing, Yunnan 655099, P.R. China

Received October 4, 2023; Accepted April 11, 2024

DOI: 10.3892/ijmm.2024.5378

Abstract. Fibroblast growth factor (FGF)21 is a peptide hormone that improves mitochondrial function and energy metabolism, and the deficiency of its co-receptor β-klotho (KLB) causes decreased FGF21 sensitivity. The present study examined whether the cardiac delivery of plasmids containing the *KLB* gene via ultrasound-targeted microbubble destruction (UTMD) enhances the efficacy of FGF21 against heart failure post-acute myocardial infarction (AMI). For this purpose, the levels of FGF21 in patients and rats with heart dysfunction post-infarction were determined using ELISA. Sprague-Dawley rats received the 3X UTMD-mediated delivery of KLB@cationic microbubbles (KLB@CMBs) 1 week following the induction of AMI. Echocardiography, histopathology and biochemical analysis were performed at 4 weeks following the induction of AMI. The results revealed that patients with heart failure post-infarction had higher serum FGF21 levels than the healthy controls. However, the downstream signal, KLB, but not α-klotho, was reduced in the heart tissues of rats with AMI. As was expected, treatment with FGF21 did not substantially attenuate heart remodeling post-infarction. It was found that decreased receptors KLB in the heart may result in the insensitivity to FGF21 treatment. *In vivo*, the UTMD technology-mediated delivery of KLB@CMBs to the heart significantly enhanced the effects of FGF21 administration on cardiac remodeling and mitochondrial dysfunction in the rats following infarction. The delivery of KLB to the heart by UTMD and the administration of FGF21 attenuated mitochondrial impairment and oxidative stress by activating nuclear factor erythroid 2-related factor 2 signals. On the whole, the present study demonstrates that the cardiac delivery of KLB significantly optimizes the cardioprotective effects of FGF21 therapy on adverse heart remodeling. UTMD appears a promising interdisciplinary approach with which to improve heart failure post-myocardial infarction.

Correspondence to: Dr Chaofu Yue or Dr Mei Yang, Department of Intensive Care Unit, Qujing First People's Hospital, 1 Garden Road, Qilin, Qujing, Yunnan 655099, P.R. China
E-mail: yueaaa0@163.com
E-mail: ym780926@qq.com

*Contributed equally

Key words: fibroblast growth factor 21, β-klotho, heart failure, acute myocardial infarction, ultrasound-targeted microbubble destruction

Introduction

Acute myocardial infarction (AMI) and subsequent heart failure (HF) remain one of the leading causes of mortality and disability worldwide (1,2). Mitochondrial dysfunction is a critical determinant of cell death in acute phases and heart remodeling in chronic phases following AMI (1). Therefore, targeting mitochondrial dysfunction may be a promising therapeutic strategy with which to mitigate cardiac remodeling (3,4).

Fibroblast growth factor (FGF)21 is a peptide hormone from the FGF protein family and is predominantly secreted by liver tissue. It plays a crucial role in the regulation of mitochondrial stress and metabolism by binding to FGF cell surface receptors and its obligatory coreceptor β-klotho (KLB) (5,6). There is evidence to suggest that increased FGF21 levels improve defective mitochondrial function and stress adaptation in muscles (7). Moreover, it has been shown that the overexpression of FGF21 significantly reduces aging-related obesity, adipose tissue hypertrophy and inflammation (8), indicating appealing prospects for the clinical translation of FGF21signaling in aging-associated metabolic diseases.

Patients with AMI manifest elevated serum FGF21 levels compared with healthy individuals, and FGF21 levels are significantly related to an increased incidence of adverse cardiovascular events at 30 days post-infarction (9). In addition, mice with diabetic cardiomyopathy have also been found

to have higher circulating levels of FGF21 than non-diabetic mice (5). Notably, exercise reduces FGF21 levels, while enhancing FGF21 sensitivity by promoting co-receptor KLB expression in heart tissues, attenuating diabetes-related cardiac pathological remodeling (5). Therefore, it was hypothesized that promoting KLB expression rather than excessively increasing FGF21 levels may more effectively mitigate cardiac remodeling post-myocardial infarction (MI).

Ultrasound-targeted microbubble destruction (UTMD) is an emerging approach for targeted delivery of drugs and gene transport to specific tissues (10). Employing low-frequency ultrasound offers the advantages of enhanced penetration, reduced attenuation and focalization on deep-seated local tissues (11). Intravenous microbubbles flow in the bloodstream and oscillate, collapsing within the target tissue under ultrasound stimulation, causing localized cavitation effects that enhance the penetration and uptake of carried plasmids (12). The UTMD technique has demonstrated efficacy and safety in gene delivery to target organs and is extensively validated in rodent and primate models (10). Furthermore, UTMD circumvents ethical and biosafety controversies associated with viral gene delivery (13), and the clinical safety of ultrasound microbubbles is widely recognized in diagnostics and therapy (14,15).

In the present study, it was hypothesized that the UTMD-targeted delivery of the KLB gene to the heart prevents the occurrence of HF post-infarction. The *KLB* gene exerts this effect by augmenting myocardial KLB expression, enhancing FGF21 sensitivity, and attenuating mitochondrial dysfunction and cardiac remodeling post-infarction through the FGF21-KLB pathway. These findings contribute to the advancements of the clinical translation of the FGF21 pathway as a promising therapeutic avenue within the cardiovascular field.

Materials and methods

Study participants. A total of 50 patients aged ≥20 years and diagnosed with HF post-infarction without renal replacement therapy were enrolled between June and December, 2022 at the Department of Cardiology of the Qujing First People's Hospital, Qujing, China. Age- and sex-matched healthy adults from the outpatient department not diagnosed with cardiovascular diseases were included as the control group. Fasting serum samples were collected and stored at -80˚C. The Ethics Review Board of Qujing First People's Hospital approved the study protocols (approval no. QJFH2021-017). All participants provided written informed consent prior to enrollment.

Animal models. A total of 100 healthy male Sprague-Dawley rats (weighing 220-250 g; 8 weeks old) were purchased from the Animal Center of Kunming Medical University and kept at ~22˚C and a 12-h light-dark cycle with free access to food and water. The study protocols were in accordance with the Guide for the Care and Use of Laboratory Animals and approved by the Animal Care and Use Committee of Kunming Medical University (Kunming, China). All relevant animal welfare considerations were taken, including efforts to minimize suffering and distress, the use of analgesics or anesthetics or special housing conditions, particularly for the AMI and UTMD procedures.

The left anterior descending coronary artery ligation was performed to induce AMI and establish a model of MI in rats, as previously described (16). An intraperitoneal injection of ML385 (30 mg/kg, HY-100523, MedChemExpress) was administered to inhibit nuclear factor erythroid 2-related factor 2 (Nrf2) activity, as previously described (17). All animals were randomly divided into the following experimental groups: The sham-operated (sham) group (n=8), the AMI group (n=36), the GFP + UTMD group (n=5), the AMI + FGF21 group (n=12), the AMI + UTMD@Vector group (n=3), the AMI + UTMD@*KLB* group (n=12), the AMI + UTMD@*KLB* + FGF21 (n=12) group and the AMI + UTMD@*KLB* + FGF21 + ML385 group (n=12). During the surgery, 5, 3, 2, 3 and 3 rats died in the AMI, AMI + FGF21, AMI + UTMD@*KLB*, AMI + UTMD@*KLB* + FGF21 and AMI + UTMD@*KLB* + FGF21 + ML385 groups, respectively, due to sudden cardiac death and severe heart failure. The mortality rate as was expected according to previous studies using rats following left anterior descending coronary artery (LAD) occlusion (18-20). Animal health and behavior were monitored every day for the first week, then once every 2 days. The pre-designed humane endpoints in the present study mainly were severe heart failure, loss of appetite and fragility for >24 h and an agonal stage. A total of 3 rats reached the humane endpoints and were therefore euthanized before the end of the study and were thus recorded as deaths due to heart failure.

In brief, the rats were placed in the supine position for endotracheal intubation and anesthetized by the inhalation of 2-3% isoflurane (induction, 3%; maintenance, 2%) using a small animal anesthesia machine (Harvard Apparatus). All animals received buprenorphine hydrochloride (0.1 mg/kg, subcutaneous injection) for pain management when establishing the model of MI. The surgical procedure involved a left thoracotomy to access the heart. A 5-0 Prolene suture with a needle was used to ligate the LAD. The ligation was performed ~2 mm below the left atrial appendage. The model of MI model was validated by observing distinct changes in the heart anatomy, and the whitening of the left ventricular anterior wall and apex. The rats in the sham group were only subjected to drilling underneath the LAD coronary artery but were not ligated. The rats were administered an intraperitoneal injection of the vehicle (0.9% saline, ST341, Beyotime Institute of Biotechnology) or FGF21 at 0.5 mg/kg/day. Recombinant human FGF21 (CSB-AP002471HU, Cusabio Technology, LLC) was expressed in *E. coli* and harvested by ion exchange and hydrophobic interaction chromatography, as previously described (21). In accordance with the AVMA Guidelines for the Euthanasia of Animals, the rats were euthanized by cervical dislocation under anesthetization with isoflurane inhalation (induction, 3%; maintenance, 2%). Animal death was verified by respiratory cessation and muscular tension disappearance. Subsequently, ~3 ml blood was rapidly obtained from the heart cavity to extract serum for use in enzyme-linked immunosorbent assay (ELISA). The heart tissues were then harvested for use in subsequent experiments. The duration of the animal experiment was 4 weeks, including the establishment of the model of AMI, the UTMD procedure and subsequent observation until euthanasia.

Cationic microbubble (CMB) generation. CMBs were synthesized using the thin-film hydration-sonic vibration method, as previously described (22). A mixture of chemicals, including dipalmitoyl-phosphatidylcholine (cat. no. 850355P-1G-A-3214, Avanti Polar Lipids, Inc.), 1,2-distearoyl-sn-glycerol-3-phosphoethanolamine-N-maleimide (DSPE-PEG, cat. no. 880160P-200MG-A-047, Avanti Polar Lipids, Inc.) and 3β-[N-(N',N'-dimethyl-aminoethane)-carbamoyl] cholesterol (DC-Chol, cat. no. 700001P-200MG-B-021, Avanti Polar Lipids, Inc.), was prepared and processed to form a thin lipid film (mass ratio, 5:2:0.5) (10). Glycerol solution (cat. no. 56-81-5, MilliporeSigma) was added, and octafluoropropane (C3F8, Foshan Huate Gas Co. Ltd.) gas was bubbled through the solution to generate gas-filled CMBs, widely used in clinical practice with favorable safety and performance (23). The CMBs were diluted to $1x10^9$/ml with PBS (C0221A, Beyotime Institute of Biotechnology), treated with ^{60}Co-γ irradiation (BFT-II Cobalt-60 gamma-ray Irradiation Device, MDS Nordion) and stored at 4˚C. The particle size distribution and surface potential were determined using the Zetasizer Nano ZS system (Malvern Panalytical Ltd.) (10).

KLB@CMB generation. Plasmids (80 μg, Hanbio Biotechnology Co., Ltd.) expressing the GFP or *KLB* gene were incubated in a 100-μl CMB suspension ($0.5x10^9$ MBs) for 15 min. The suspension was centrifuged at 400 x g for 5 min under 4˚C to obtain plasmid-bound CMBs (10). The percentage of bound plasmid DNA and the payload mass of plasmid DNA in CMBs were calculated as follows: Percentage of bound plasmid DNA in CMBs=(DNA_{total}-DNA_{free})/DNA_{total} x100%; payload mass of plasmid DNA in CMBs=(DNA_{total}-DNA_{free})/CMB number (10). The plasmid DNA was stained by 10 μg/ml propidium iodide solution (C0080 Beijing Solarbio Science & Technology Co., Ltd.) for 10 min at room temperature. The combination of plasmid DNA and CMBs was validated using a fluorescence microscope (DMI3000, Leica Microsystems GmbH) and a flow cytometer (BD Biosciences).

UTMD technology. All animals were anesthetized via isoflurane inhalation (induction, 3%; maintenance, 2%) for the UTMD procedure. In brief, the rats were administered intravenous injections of *KLB*@CMBs (1.0-1.2 ml/h) via the tail vein, as previously reported (10). An M3S transducer (S5-1 probe, GE Healthcare) with a low 1-5 MHz frequency range was used due to the known 1-3 MHz resonant frequency of microbubbles (10,12,24). The parameters of the second harmonic mode were used and set as transmit 1.6 MHz and receive 3.2 MHz, mechanical index (MI, low 0.30; flash, 1.31), and -16 dB output power (10). The *KLB* delivery to the heart was repeated three time at 1-day intervals at 1, 3, and 5 days at 1 week following the induction of AMI (25).

Rat cardiomyoblast H9C2 cell culture and treatment. H9C2 rat cardiomyoblasts (purchased from The Cell Bank of Type Culture Collection of the Chinese Academy of Sciences) were cultured in DMEM containing 10% (v/v) fetal bovine serum (cat. no. 0500, ScienCell Research Laboratories, Inc.) in a humidified incubator with 5% CO_2 and at 37˚C. When the cell density reached 60%, the cells were transfected with a plasmid containing the *KLB* gene using Lipofectamine 3000® reagent (L3000008, Invitrogen; Thermo Fisher Scientific, Inc.) following the manufacturer's protocols. The cells were cultured with or without FGF21 (2 μg/ml, CSB-AP002471HU, Cusabio Technology, LLC) for 24 h. Subsequently they were treated under hypoxic conditions (5% CO_2 and 1% O_2 at 37˚C) to mimic AMI for 4 h and collected for further analysis.

Echocardiography assessment. As previously described, cardiac function was evaluated using an M-mode echocardiography system (S12-4 probe, EPIQ 5; Koninklijke Philips N.V.) 4 weeks following the induction of AMI (16). The rats were lightly anesthetized via isoflurane inhalation (induction, 3%; maintenance, 1.5%) for the echocardiography assessment. Left ventricular end-systolic diameter (LVESD) and left ventricular end-systolic diameter (LVESD) were measured to calculate the left ventricular ejection fraction (LVEF) and left ventricular fractional shortening (LVFS) using computer algorithms. Each diameter was obtained from at least four consecutive cardiac cycles and averaged.

Cell death assessment. To evaluate the apoptosis of H9C2 cells or that of cells in the heart sections, terminal deoxynucleotidyl transferase-mediated dUTP nick-end labeling (TUNEL) staining (cat. no. A321, Elabscience) was used, as previously described (3). The apoptotic index was calculated by determining the ratio of TUNEL-positive nuclei to the total nuclei counts in five randomly selected fields per sample, as previously described (10).

Assessment of reactive oxygen species (ROS) generation. For the assessment of ROS generation DHE staining was performed on fresh heart tissues (10). The heart sections were pre-treated with cold PBS for 10 min and exposed to 10 μmol/l DHE solution (cat. no. S0063, Beyotime Institute of Biotechnology) at 37˚C in a dark environment, as previously described (10). Following a 30-min incubation at 37˚C, the heart sections were subjected to triple PBS washes and were maintained in a wet condition until examination through a fluorescence microscope (Leica Microsystems GmbH).

Assessment of mitochondrial membrane potential. Mitochondrial membrane potential was determined using the JC-1 staining assay kit (cat. no. C2005, Beyotime Institute of Biotechnology), as previously described (26). JC-1, a fluorescent dye, accumulated in the mitochondrial matrix in two forms: Aggregates (red fluorescence) in polarized mitochondria and monomers (green fluorescence) in depolarized mitochondria (10). The heart sections were treated with 10 μg/ml JC-1 solution at 37˚C for 0.5 h in a light-protected environment, as previously described (27). Following three washes with PBS, the fluorescence intensity was observed using a fluorescence microscope (Leica Microsystems GmbH). To quantify the mitochondrial membrane potential, five random images were captured per sample and the fluorescence intensity of both the J-monomers and the J-aggregates was examined.

Assessment of mitochondrial respiratory function. As previously described (28), the H9C2 cells were intervened and digested with pancreatic enzymes, and the cell suspension

was then collected for analysis. The mitochondrial respiratory function was assessed using an XF24 Extracellular Flux Analyzer (Seahorse Bioscience) with a sequential titration of oligomycin, carbonyl cyanide 4-(trifluoromethoxy) phenylhydrazone (FCCP), rotenone and antimycin A (XF Cell Mito Stress Test kit, Seahorse Bioscience), as previously described (28).

Assessment of antioxidant capacity. Total antioxidant capacity was measured using a commercial kit based on the ferric-reducing ability of plasma method (S0116, Beyotime Institute of Biotechnology) according to the product manual. The capacity was quantified by measuring the absorbance at 593 nm using a microplate reader (Infinite F500, Tecan Group, Ltd.) and estimated as a percentage of the combined ferric reducing/antioxidant potency of the antioxidants in protein.

Pathological analysis. The heart tissues were fixed with 4% paraformaldehyde (cat. no. P0099, Beyotime Institute of Biotechnology) at room temperature for 72 h and subsequently sliced into sections measuring 5 μm in thickness. These sections were subjected to staining with hematoxylin and eosin [H&E; Right Tech, China] for 2 min at room temperature, and Masson's Trichrome Stain with celestine blue staining (cat. no. G1346, Beijing Solarbio Science & Technology Co., Ltd.) for 3 min at room temperature and Ponceau-acid magenta staining (cat. no. C0189, Beyotime Institute of Biotechnology) for 10 min at room temperature to observe and analyze the cardiac fibrosis morphology using microscope (Olympus IX70, Olympus Corporation) according to the manufacturer's instructions.

Cell viability assay. The MTT Cell Proliferation Assay kit (cat. no. C0009, Beyotime Institute of Biotechnology) was used to assess cell viability. The H9C2 cells ($0.5x10^4$ per well) were cultured in 96-well plates and treated as needed (e.g., plasmid transfection, FGF21 treatment and hypoxia-induced stress), and were then incubated with MTT reagent for 4 h at 37˚C (10). Additionally, lactate dehydrogenase (LDH) activity was measured in the serum or medium supernatant using a commercially available assay kit (cat. no. A020, Jiancheng Bioengineering Institute). A total of 50 μl diluted serum was added to 96-well plates and combined with 50 μl reaction mix [the mixed solution of reagent I and II (v/v: 5:1)] per well (10). The absorbance was then measured at 450 nm using a spectrophotometer (Evolution 60S, Thermo Fisher Scientific, Inc.), and LDH activity was calculated following the manufacturer's instructions (10).

ELISA. The serum levels of creatine kinase-myocardial band (CK-MB; E-EL-R1327c, Elabscience Biotechnology Co., Ltd.), cardiac troponin T (cTnT; E-EL-R0151c Elabscience Biotechnology Co., Ltd.), KLB (ml028418, Mlbio) and FGF21 (CSB-EL008627RA, Cusabio Biotechnology Co., Ltd.) were measured according to the instructions provided with the kits.

Reverse transcription-quantitative PCR (RT-qPCR). Total RNA was extracted using TRIzol reagent (cat. no. B0201, HaiGene) and converted into cDNA using the RT Easy II First Strand cDNA Synthesis kit (cat. no. 04379012001, Roche Diagnostics), as previously described (16). Followinh incubation for 60 min at 42˚C, the reactions were terminated by heating at 70˚C for 10 min. qPCR was performed using the Real-Time PCR Easy (HY-K0501SYBR-Green I, MedChemExpress), with the following procedures: Denaturation at 95˚C for 10 min, amplification by 40 cycles of 95˚C for 10 sec and 60˚C for 30 sec. Gene expression was normalized to β-actin and calculated using the $2^{-\Delta\Delta cq}$ method (29). The primer sequences are presented in Table SI.

Western blot analysis. Total proteins were extracted from the H9C2 cells or heart tissues using RIPA buffer containing protease (P0013C, Beyotime Institute of Biotechnology) and phosphatase inhibitors (P1045, Beyotime Institute of Biotechnology). The protein concentration was determined using BCA assay. Specifically, ~30 μg proteins per lane were loaded into 10% SDS-PAGE gels and transferred onto 0.22 μm PVDF membranes (MilliporeSigma). The membranes were blocked using 5% BSA (ST025, Beyotime Institute of Biotechnology) for 1 h at room temperature, and incubated using corresponding primary antibodies overnight at 4˚C and HRP-linked secondary antibody for 1 h at room temperature (all antibodies used are listed in Table SII). Due to the close molecular weights of the target proteins, the protein expression signals on different membranes were detect with the same loading amount, and all other western blotting conditions for each protein were also the same excepting the primary antibody used. The density of immunoreactivity was assessed using a chemiluminescence ECL kit using a chemiluminescence system (Tanon 5200, Tanon Science & Technology Co., Ltd.) (30). ImageJ software (version v1.52a, National Institutes of Health) was used for the semi-quantification of protein expression.

Statistical analyses. Unless stated otherwise, quantitative variables are expressed as the mean ± standard deviations (SD). Statistical analyses and data visualization were conducted using SPSS 20.0 software (IBM Corp.) and GraphPad Prism (version 6.0; Dotmatics). The Shapiro-Wilk test was used to evaluate data distribution, and $P>0.05$ was considered as passing the normality test. As the clinical data in Fig. 1A did not meet the normal distribution ($P<0.001$ in the Shapiro-Wilk test), the non-parametric Mann-Whitney U test was adopted for the comparison of two groups here. Following normality tests, a two-tailed unpaired Student's t test was conducted for the comparisons of two groups, and one-way ANOVA with Tukey's post hoc test were used for the comparisons of multiple groups. The correlation between FGF21, KLB and myocardial injury biomarkers was examined using Spearman's correlation analysis. A P-value <0.05 was considered to indicate a statistically significant difference.

Results

FGF21 levels are increased, but FGF21 sensitivity is decreased in the heart post-infarction. The serum levels of FGF21 were measured in patients with HF following MI and in age- and sex-matched healthy participants. The serum levels of FGF21 in the patients with HF were significantly increased compared with those in the healthy participants (128 vs. 111 pg/ml,

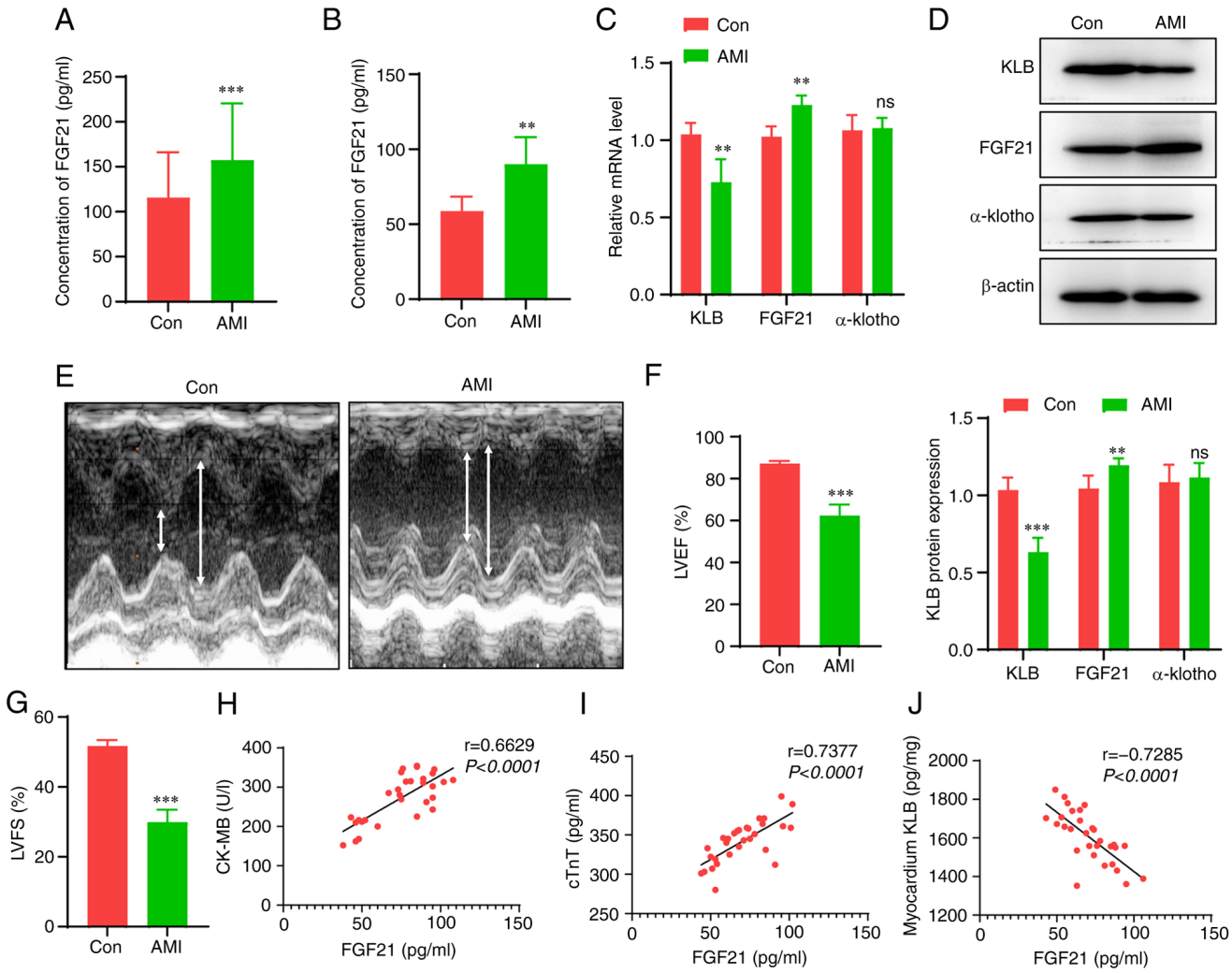

Figure 1. Serum FGF21 and its receptor KLB in humans and rats post-infarction. (A) Serum levels of FGF21 in patients with AMI, and age- and sex-matched healthy controls (n=50). (B) Serum levels of FGF21 in rats post-infarction (n=5). (C) Relative mRNA levels of KLB receptors in heart tissue (n=5). (D) Relative protein levels of KLB, FGF21 and α-klotho in heart tissue (n=5). (E) Representative images of echocardiography (n=5). (F) Measurements of LVEF (n=5). (G) Measurements of LVFS (%) (n=5). (H) Spearman's correlation analyses between CK-MB and serum levels of FGF21 (n=30). (I) Spearman's correlation analyses between cTnT and serum levels of FGF21 (n=30). (J) Spearman's correlation analyses between cTnT and KLB levels (n=30). **P<0.01 and ***P<0.001 vs. the control (Con) group; ns, not significant. KLB, β-klotho; FGF21, fibroblast growth factor 21; AMI, acute myocardial infarction; LVEF, left ventricular ejection fraction; LVFS, left ventricular fractional shortening.

Fig. 1A). Subsequently, AMI was induced in rats to provoke HF and the FGF21 serum levels were measured. Consistent with the results obtained in the patients, the rats with HF had higher serum levels of FGF21 compared with the control rats (Fig. 1B). However, the cardiac expression of the FGF21 receptor, KLB, not α-klotho, was significantly decreased in the rats with AMI compared with the sham-operated rats (Fig. 1C and D). The successful establishment of the murine model of MI was verified by measuring the decreased LVEF and LVFS according to the echocardiography (Fig. 1E-G). Furthermore, the correlation between the severity of myocardial injury and FGF21 or KLB levels was assessed (Fig. 1H-J). Although the levels of the markers of myocardial injury, CK-MB and cTnT positively correlated with the serum levels of FGF21 (r=0.663 and 0.738, respectively), there was an inverse correlation between the cardiac KLB content and the serum levels of FGF21 (r=-0.729). These data suggest that although the FGF21 levels significantly increase following AMI, the levels of its downstream KLB co-receptor in heart tissue are markedly decreased, which may be a critical factor that decreases the cardiac response to FGF21. Hence, promoting FGF21 sensitivity may be a potential strategy with which to enhance the therapeutic efficacy of FGF21.

Overexpression of KLB enhances the protective effects of FGF21 treatment on hypoxia-induced cardiomyocyte injury in vitro. There is evidence to indicate that FGF21 activates intracellular protection signals against hypoxia-induced cellular injury (9). However, our previous observation suggests that the insufficiency of the cardiac KLB co-receptor may impair the pharmacological action of FGF21 (Fig. 1C and D). Further experiments were performed. First, the transfection of plasmid containing the *KLB* gene significantly induced KLB overexpression in H9C2 cells under normal conditions or hypoxia, as verified by measuring its mRNA and protein levels (Fig. S1). As was expected, the cellular activity of H9C2 cells decreased after 3 h under hypoxic conditions *in vitro* (Fig. 2A). However, FGF21 treatment or KLB overexpression alone

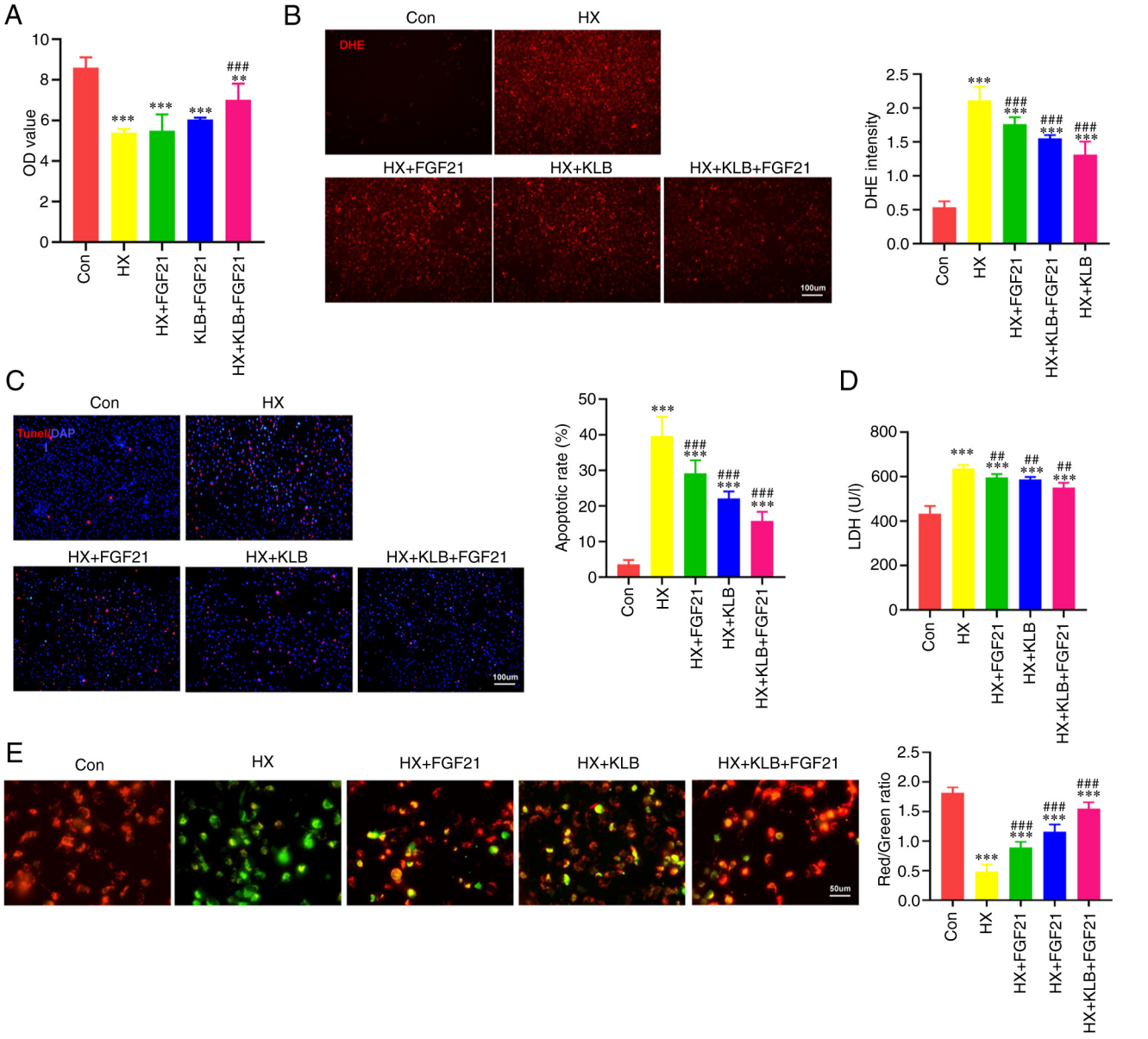

Figure 2. KLB overexpression enhances the protective effects of FGF21 treatment on hypoxia-induced cardiomyocyte injury *in vitro*. (A) Viability of H9C2 cells exposed to hypoxia (HX), FGF21 and KLB overexpression (n=5). (B) Representative images of DHE staining (scale bar, 100 μm), and DHE intensity was quantified to reflect ROS levels. (C) Representative TUNEL staining images of KLB-overexpressing H9C2 cells exposed to hypoxia and treated with FGF21 (n=4; scale bar, 100 μm). (D) LDH leak from KLB-overexpressing H9C2 cells exposed to hypoxia and treated with FGF21 (n=8). (E) JC-1 staining of H9C2 cells (scale bar, 50 μm). Mitochondrial membrane potential was estimated by the ratio of JC-1 aggregates (red, healthy mitochondria) and JC-1 monomers (green, depolarized mitochondria, n=5). **P<0.01 and ***P<0.001 vs. the control (Con) group; $^{\#\#}$P<0.01 and $^{\#\#\#}$P<0.001 vs. hypoxia (HX). KLB, β-klotho; FGF21, fibroblast growth factor 21; AMI, acute myocardial infarction; LDH, lactate dehydrogenase.

could not substantially reverse the decreased cellular activity of H9C2 cells under hypoxic conditions. When the cells overexpressing *KLB* were treated with FGF21, cellular injury was reduced (Fig. 2A). The present study also assessed oxidative stress, LDH leakage, and cell death that reflect hypoxia-induced myocardial injury. The overexpression of KLB enhanced the effects of FGF21, reducing ROS generation and cell injury induced by hypoxia (Fig. 2B-D). As shown by JC-1 staining, the hypoxia-induced decrease in the mitochondrial membrane potential was partly attenuated by FGF21 treatment, and KLB overexpression significantly enhanced the protective effects of FGF21 on the mitochondria (Fig. 2E). In summary, these findings suggest that KLB overexpression optimizes the effects of FGF21 on cardiomyocytes in response to hypoxia *in vitro*.

Generation and characterization of KLB@CMBs. CMBs were synthesized to carry plasmids expressing the *KLB* gene according to published procedures (10) (Fig. 3A). Dynamic light scattering revealed that he CMBs had a particle diameter of 1,482±303 nm and a zeta potential of +24.2±4.5 mV (Fig. 3B). The carrying capacity of the CMBs for the plasmids was estimated by the addition of 40 μg plasmid DNA to the CMBs, revealing the maximized carrying capacity of $0.5x10^9$/CBMs (Fig. 3C). Fluorescence microscopy revealed the stabilized *KLB*@CMBs with the *KLB*-expressing plasmid labeled by propidium iodide (Fig. 3D). According to the results of flow cytometric analysis, the binding rate of CMBs to the plasmid reached 55.2% (Fig. 3E). The synthesized *KLB*@CMBs that were prepared had a good stability within at least

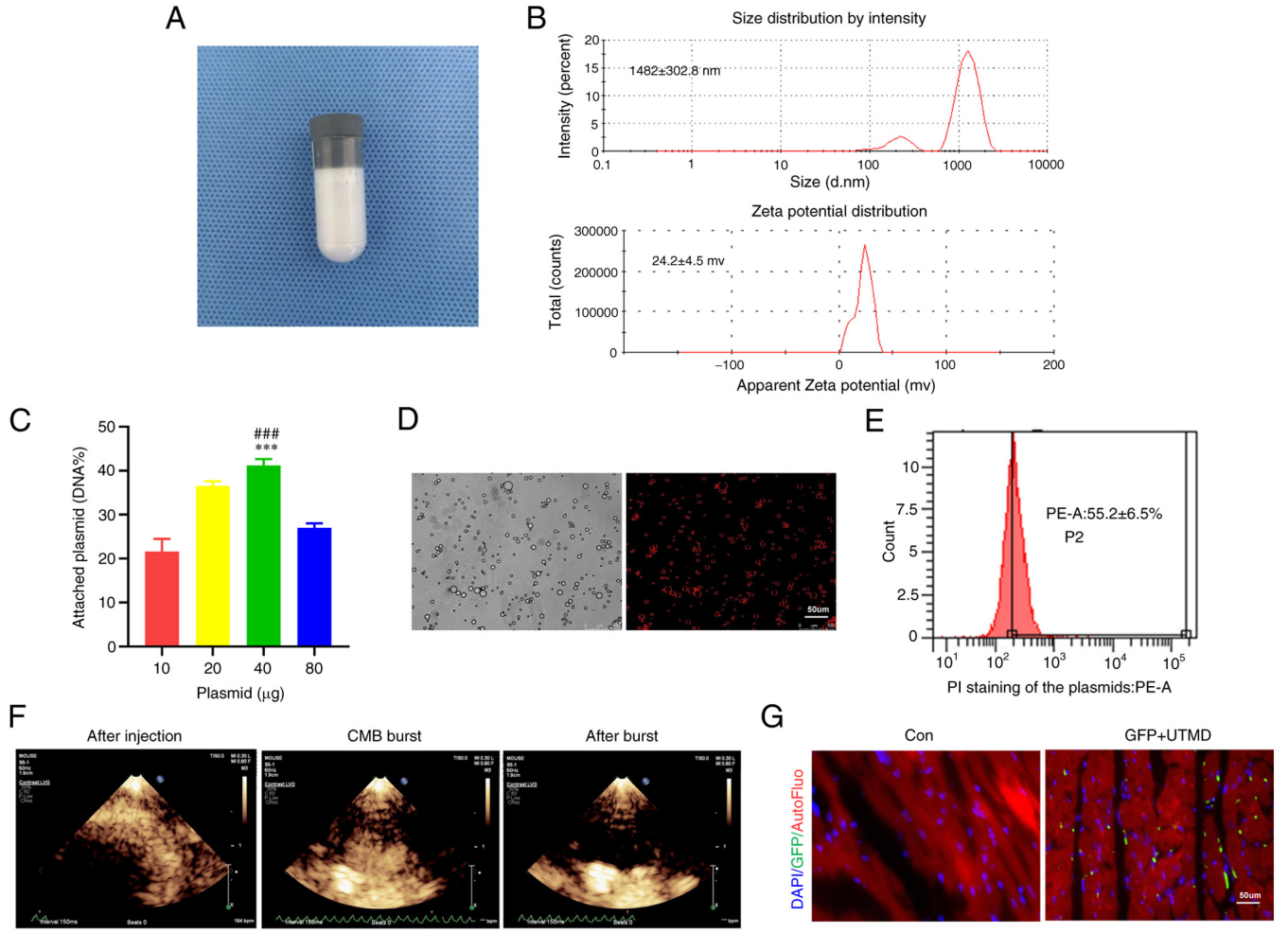

Figure 3. Assessment of plasmid@CMB preparation and delivery efficiency via UTMD technology. (A) The preparation of CMB particles. (B) Size and potential distribution of the CMBs. (C) The binding rates of several doses of plasmid on CMBs (n=4). (D) Representative images of KLB@CMBs. KLB plasmid labeled by PI staining (red) and the outline of CMB (bright) are shown (scale bar, 50 μm). (E) The binding rates of KLB@CMBs were assessed using flow cytometry (n=4). (F) Typical ultrasound contrast images of KLB@CMBs in the heart before injection, at ultrasound-targeted CMB blast, and after the CMB blast. After the CMB injection, microbubbles with high-echo intensity filled the ventricle chambers and wall tissue. The second harmonic mode with an electrocardiograph-mediated trigger was applied to activate microbubble bursting, and then only a small number of microbubbles remained and showed a low echo shadow. (G) Fluorescence images of GFP expression after plasmid containing GFP gene delivered by UTMD technique (DAPI for nucleus; green for GFP; scale bar, 50 μm). and ***P<0.001 vs. the control (Con) group; and $^{###}$P<0.001 vs. 20 μg plasmid. CMB, cationic microbubble; UTMD, ultrasound-targeted microbubble destruction; KLB, β-klotho; FGF21, fibroblast growth factor 21.

6 h under room temperature (Fig. S2). The distribution of CMBs was visualized in the heart with echocardiography, demonstrating that the UTMD-triggered CMBs burst and released the *KLB*-expressing plasmid in myocardial tissue (Fig. 3F). At 1 week after the UTMD-mediated *KLB* delivery, GFP fluorescence was detected in the heart tissue (Fig. 3G). These data confirm that the UTMD delivery of the *KLB* gene to the heart is feasible and appropriate for use in following experiments.

Combined cardiac delivery of KLB@CMBs and FGF21 administration attenuate heart remodeling. At 1 week after establishing the rat model of MI, the UTMD-mediated *KLB* delivery was repeated to the heart tissues three times. Subsequently, cardiac KLB expression was assessed, revealing that the UTMD technique significantly increased the KLB protein levels in myocardial tissue (Fig. 4A). In addition, cardiac structure and function were examined using echocardiography at 4 weeks following the induction of MI to determine whether the UTMD-mediated *KLB* delivery affects cardiac remodeling. Indeed, while the intravenous administration of FGF21 did not significantly improve LVEF and LVFS in the rats post-MI, the UTMD-mediated cardiac delivery of *KLB* significantly enhanced these parameters, amplifying the effects of FGF21 on heart dysfunction (Fig. 4B and C). Moreover, H&E staining revealed that the infarct border zone exhibited an improved tissue structure and lower injury scores in the FGF21-treated rats with *KLB*@CMBs delivered by UTMD (Fig. 4D and E). Masson's staining was also performed on the cardiac sections to evaluate the effects of combined treatment with FGF21 and the UTMD-mediated *KLB* delivery on the degree of fibrosis. The administration of FGF21 alone did not significantly reduce the infarct size, while the cardiac-specific *KLB* delivery partially improved collagen fiber alignment in the infarct area (Fig. 4F and G). These data indicated that the overexpression of KLB in the heart using the UTMD technique increased FGF21 sensitivity and attenuated adverse ventricular remodeling following MI.

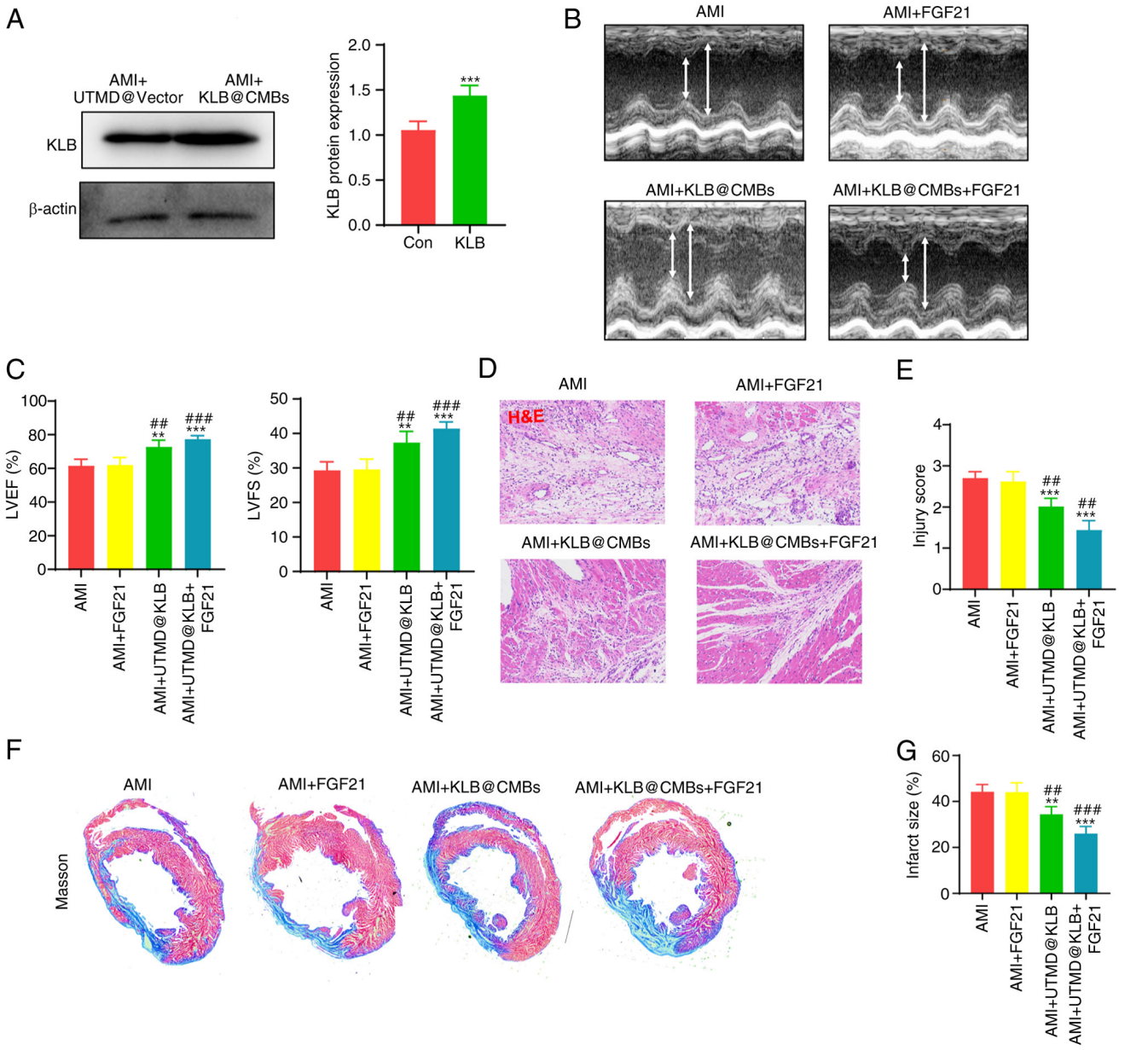

Figure 4. KLB@CMBs amplify FGF21 treatment, improving heart dysfunction and the infarction area in rats post-AMI. (A) UTMD mediated the overexpression of cardiac KLB in rats post-infarction repeated at one-day intervals 3 times. ***P<0.001 vs. the control (Con) group. (B) Representative images of echocardiography at 4 weeks after AMI surgery. (C) The LVEF and LVFS (n=5-6). (D) Representative hematoxylin and eosin-stained images of heart sections (scale bar, 100 μm). (E) Injury scores assessed according to hematoxylin and eosin images (n=5-6). (F) Representative images of Masson's staining were conducted to assess myocardial fibrosis. (G) The relative area of myocardial fibrosis was estimated according to Masson's staining (n=5-6). **P<0.01 and ***P<0.001 vs. AMI; ##P<0.01 and ###P<0.001 vs. the AMI + FGF21 group. AMI, acute myocardial infarction; KLB, β-klotho; FGF21, fibroblast growth factor 21; CMB, cationic microbubble; LVEF, left ventricular ejection fraction; LVFS, left ventricular fractional shortening.

Combined KLB@CMB delivery and FGF21 administration reduce oxidative stress and mitochondrial dysfunction in heart tissue post-infarction. Previous research has demonstrated that FGF21 regulates mitophagy, mitochondrial dynamics and mitochondrial metabolism to alleviate mitochondrial stress injury (4). Therefore, the present study examined whether the FGF21 regulation of mitochondrial function is dependent on KLB in myocardial tissue. As shown by DHE staining, whereas the administration of FGF21 did not significantly decrease myocardial ROS generation, the *KLB* gene delivery to the heart markedly reinforced the effects of FGF21 on myocardial ROS production post-infarction (Fig. 5A). In agreement with this finding, KLB expression was not affected by FGF21 administration alone (Fig. 5B). Enhanced ATP generation reflects the re-establishment of mitochondrial energy homeostasis impaired by mitochondrial dysfunction post-infarction. As was expected, treatment with FGF21 slightly recovered the ATP levels in the heart tissues, while the UTMD-mediated *KLB* delivery significantly increased the ATP generation post-infarction (Fig. 5C). Hence, KLB overexpression, but not FGF21 administration, recovered cardiac ATP production following AMI, and the combined interventions largely improved mitochondrial energy. On the whole, these data indicated that the UTMD-mediated cardiac delivery of *KLB* promoted FGF21 sensitivity, recovering mitochondrial homeostasis and alleviating adverse cardiac remodeling.

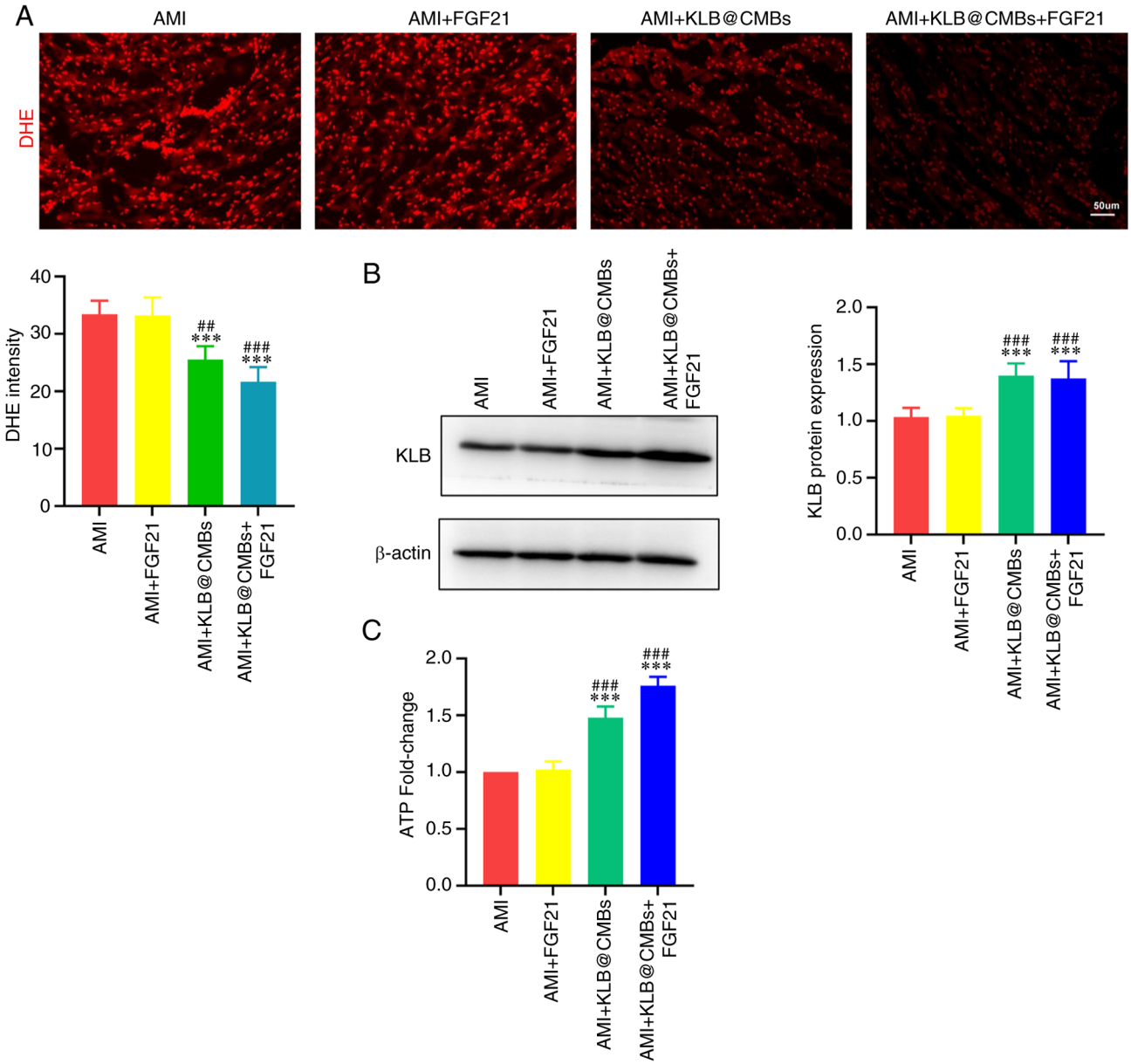

Figure 5. The combination of KLB@CMBs and FGF21 treatment inhibits myocardial oxidative stress compared with the use of FGF21 alone in rats post-infarction. (A) DHE staining in the heart sections (scale bar, 100 μm). (B) Western blot analysis and quantification of KLB expression in the heart post-infarction with or without KLB delivery and FGF21 administration. (C) ATP generation in heart tissues. ***P<0.001 vs. AMI; $^{\#\#}$P<0.01 and $^{\#\#\#}$P<0.001 vs. the AMI + FGF21 group. AMI, acute myocardial infarction; KLB, β-klotho; FGF21, fibroblast growth factor 21; CMB, cationic microbubble.

FGF21 improves mitochondrial quality via KLB/NRF2 signals to prevent the progression of heart failure following AMI. The present study then aimed to investigate how the combined FGF21 and KLB interventions mitigate oxidative stress and safeguard mitochondria post-infarction. Nrf2 antioxidant signaling is a critical protective pathway against intracellular oxidative injury (10). Thus, the present study assessed whether combined FGF21 and *KLB*@CMBs activate the Nrf2-mediated antioxidant pathway to improve heart dysfunction. Indeed, FGF21 administration and *KLB* delivery significantly sensitized the heart to FGF21 treatment and increased Nrf2 expression, which was inhibited by ML385, an NRF2 inhibitor (Fig. 6A). By contrast, the protein expression of kelch-like ECH-associated protein 1 (KEAP1), an inhibitor of Nrf2 binding, did not significantly decrease after the combined FGF21 and *KLB* interventions (Fig. 6A). Therefore, the combined interventions may prevent heart failure post-infarction by promoting Nrf2 expression and not reducing KEAP1 expression (Fig. 6A). As was expected, *KLB* delivery and FGF21 treatment increased the expression of the Nrf2 target proteins, heme oxygenase 1 (HO-1), NAD(P)H quinone dehydrogenase 1 (NQO1) and glutamate-cysteine ligase modifier subunit (GCLM) (Fig. 6B). Conversely, the Nrf2 inhibitor, ML385, significantly abolished these effects and reduced the expression of these antioxidant enzymes (Fig. 6B). Furthermore, it was verified that the ML385 injection significantly reduced the protective effects of combined FGF21 and *KLB*@CMB treatment on cardiac dysfunction in rats post-infarction (Fig. 6C-E). Finally, DHE staining was performed to assess superoxide anion free radicals,

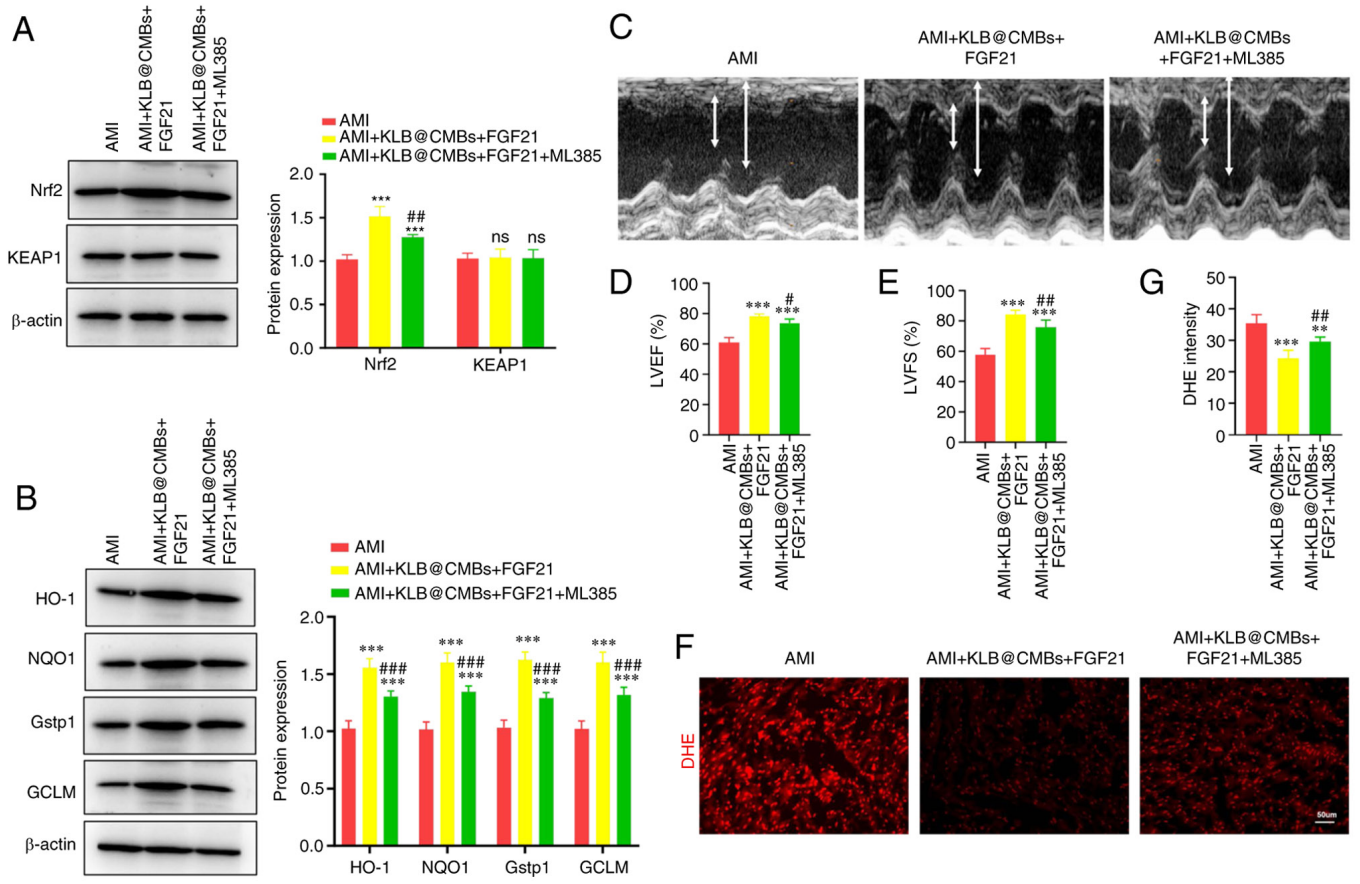

Figure 6. Cardiac delivery of KLB enhances the antioxidant effects of FGF21 in the heart following AMI. (A) Western analysis and quantification of Nrf2 and KEAP1 expression in H9C2 cells (n=4). (B) The protein expression of HO-1, NQO1, Gstp1 and GCLM was assessed using western blot analysis (n=4). (C) Representative images of echocardiography at 4 weeks following AMI surgery. (D and E) The LVEF and LVFS were calculated (n=5). (F and G) DHE staining of the heart section (scale bar, 50 μm) and quantification (n=5). **P<0.01 and ***P<0.001 vs. AMI; $^{\#}$P<0.05, $^{\#\#}$P<0.01 and $^{\#\#\#}$P<0.001 vs. the AMI + KLB@cMBs + FGF21 group; ns, not significant. AMI, acute myocardial infarction; KLB, β-klotho; FGF21, fibroblast growth factor 21; CMB, cationic microbubble; LVEF, left ventricular ejection fraction; LVFS, left ventricular fractional shortening; Nrf2, nuclear factor erythroid 2-related factor 2; KEAP1, kelch-like ECH-associated protein 1; HO-1, heme oxygenase 1; NQO1, NAD(P)H quinone dehydrogenase 1; Gstp1, glutathione S-transferase pi-1; GCLM, glutamate-cysteine ligase modifier subunit.

demonstrating that oxidative stress was moderately attenuated by *KLB* cardiac delivery, and the Nrf2 inhibitor compromised the antioxidant effect of KLB in the heart post-infarction (Fig. 6F and G). Moreover, the total antioxidant capacity in the heart tissues increased by the combination of FGF21 and *KLB*@CMB treatment was attenuated by the inhibition of Nrf2 (Fig. S3).

The present study further evaluated the effects of Nrf2 inhibition and the FGF21-KLB-mediated activation on mitochondrial quality. The combined interventions improved the loss of mitochondrial membrane potential in the myocardial tissues post-infarction, and this effect was attenuated by the inhibition of Nrf2 (Fig. 7A and B). The mitochondrial transmembrane potential reflects mitochondrial function and impaired mitochondria are the primary source of ROS production. The mitochondrial oxygen consumption rate (OCR) revealed that FGF21-KLB boosted the basal respiration level, partly reduced by Nrf2 inhibitor treatment in the H9C2 cardiomyoblasts (Fig. 7C). In addition, the synthetic compound, FCCP, uncoupled mitochondria respiration from oxidative phosphorylation, indicating a similar difference in the measurement of maximal OCR (Fig. 7C-G). These results imply that combined GFG21-KLB interventions improve mitochondrial function in H9C2 cardiomyoblast cells under hypoxic conditions, and this effect is compromised by Nrf2 inhibition.

Discussion

The FGF21 signaling pathway improves insulin resistance and mitigates mitochondrial stress, exerting a protective effect on cardiometabolism (8). However, little is known about how to translate FGF21-targeted interventions into clinical practice for preventing adverse remodeling. In the present study, it was discovered that serum FGF21 levels increased, but cardiac KLB levels decreased following MI infarction in rats. The co-receptor KLB-dependent pathway was essential for the protective effects of FGF21 on cardiac adverse remodeling post-infarction. Cardiac KLB delivery using UTMD technology markedly upregulated KLB protein expression in heart tissues, sensitizing the myocardium to FGF21 and optimizing its therapeutic effect in rats with AMI beyond FGF21 intervention alone. Our findings offer novel insights into the translation of FGF21 therapy in cardiac remodeling. Moreover, the FGF21-KLB pathway was identified as a promising target with which to prevent HF following

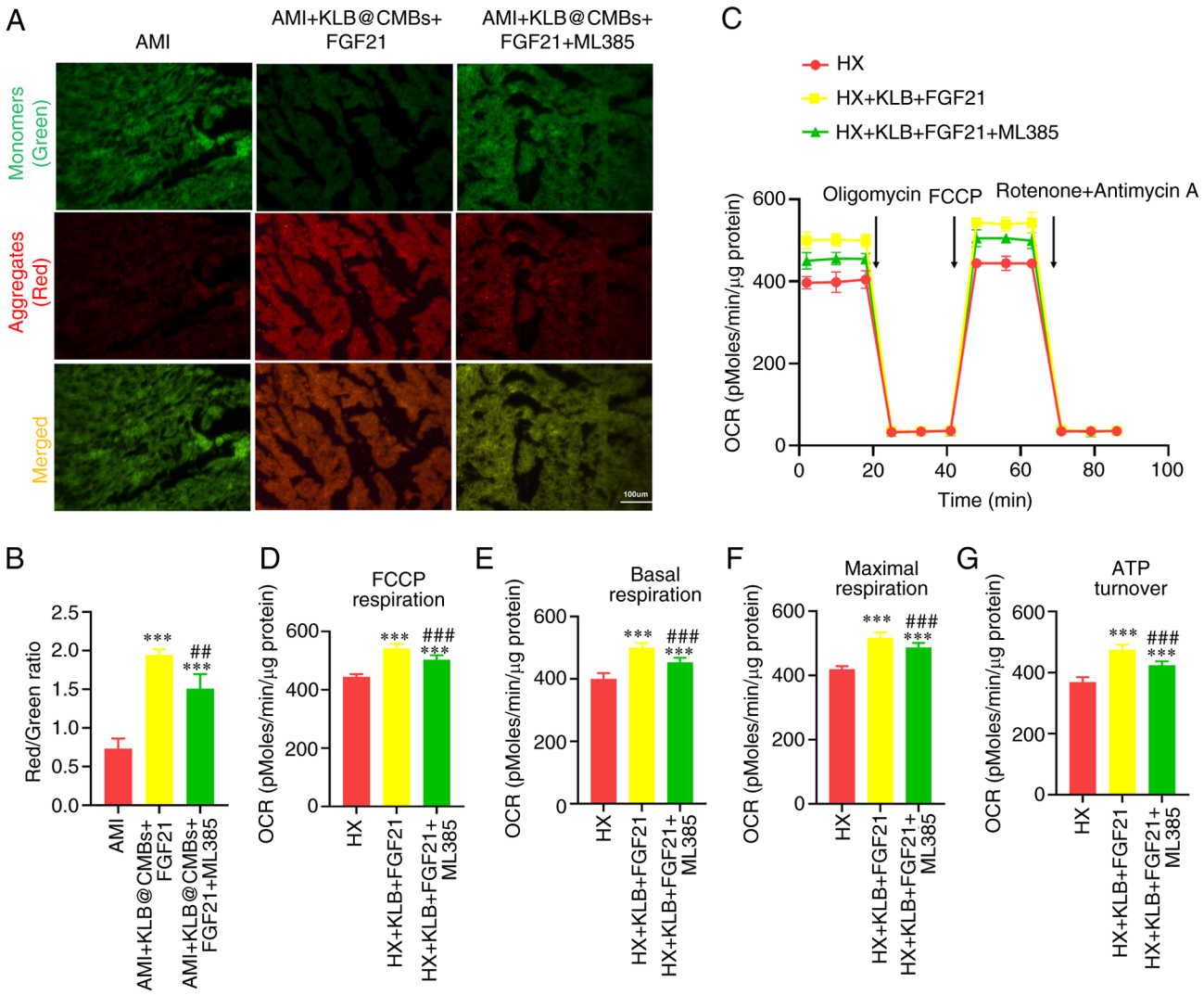

Figure 7. Mitochondrial quality in the heart is improved by the UTMD-mediated KLB delivery and FGF21 treatment in rats post-infarction. (A) JC-1 staining of heart section post-infarction (scale bar, 100 μm). (B) The ratio of JC-1 aggregates (red) and monomers (green) was used to assess mitochondrial membrane potential (n=5-6). (C) Mitochondrial OCR profile in H9C2 cells using an XF24 Extracellular Flux Analyzer. Oligomycin (1 μmol/l), FCCP (4 μmol/l) and rotenone (0.5 μmol/l) plus antimycin A (0.5 μmol/l) were added sequentially. (D) FCCP-related respiration, (E) basal respiration, (F) maximal respiration and (G) ATP turnover were calculated (n=4). ***P<0.001 vs. AMI; $^{\#\#}$P<0.01 and $^{\#\#\#}$P<0.001 vs. the AMI + KLB@CMBs + FGF21 group. CMB, cationic microbubble; UTMD, ultrasound-targeted microbubble destruction; KLB, β-klotho; FGF21, fibroblast growth factor 21; OCR, oxygen consumption rate; FCCP, carbonyl cyanide 4-(trifluoromethoxy) phenylhydrazone; AMI, acute myocardial infarction; HX, hypoxia.

MI by alleviating mitochondrial dysfunction and oxidative stress via Nrf2 activation.

There is evidence to indicate the promising potential of FGF21 administration in addressing cardiometabolic disorders, such as obesity, diabetes and ageing (5,6,8,31). Herein, significantly elevated serum levels of FGF21 were observed in rats post-infarction, consistent with previous reports that serum FGF21 levels paradoxically increase in diabetes and its cardiovascular complications (9,32). Hence, the increased serum levels of FGF21 and the decreased expression of KLB following MI may reflect a compensatory response to FGF21 resistance (5). Similarly, cardiac remodeling or HF is accompanied by the elevated expression of natriuretic peptides, suggesting that the intravenous injection of natriuretic peptides could also provide additional benefits to improve HF symptoms (33). The findings of the present study and those of other studies suggest that the targeted restoration of cardiac KLB expression significantly promotes the activation of FGF21 receptor-dependent pathways in rats post-MI, closely associated with improvements in cardiometabolic parameters, suggesting an increase in FGF21 sensitivity (5,34). Treadmill exercise substantially induces cardiac KLB expression, enhancing cardiomyocyte responsiveness to FGF21 and reinforcing its therapeutic effect on the diabetic heart in rat models (5). The present study demonstrated that FGF21 treatment alone had limited preventive effects on HF post-infarction, as FGF21 supplementation failed to reverse mitochondrial dysfunction and cardiac remodeling. Notably, the therapeutic effectiveness of FGF21 against cardiac dysfunction was markedly augmented by the UTMD-mediated cardiac *KLB* delivery. As patients in the recovery phase post-infarction may not endure high-intensity exercise (35), the impact of moderate- to low-intensity exercise on cardiac KLB expression remains unclear. Nonetheless, the present study provides a feasible approach for preventing HF progression post-infarction. The findings indicate that the cardiac-targeted *KLB* delivery may enhance the FGF21 pathway, conferring the

protective effects of FGF21 administration on cardiomyocytes. In summary, following AMI, UTMD-mediated delivery to the heart reprograms it into a target organ responsive to FGF21 by strengthening its receptor-dependent pathway (8), promoting the protective effects of FGF21 administration on myocardial tissues.

Dysfunctional mitochondria are the primary sites of ROS generation and oxidative stress in the heart post-infarction, playing a crucial role in the pathological progression of adverse cardiac remodeling (30). Mitochondrial dysfunction and structural abnormalities are observed in several common types of heart diseases, including hypertrophic cardiomyopathy, diabetic cardiomyopathy and tumor-related cardiac injury (36). These disorders are strongly associated with abnormalities in cardiac energy metabolism, a decreased ATP production and deteriorating cardiac function (1,5). Mitochondrial structural anomalies and elevated levels of oxidative stress have been observed in cardiac biopsies from patients with MI (1). In the present study, in rat hears post-MI, significant mitochondrial functional abnormalities, excessive ROS production and a disrupted energy homeostasis were observed. These features were reversed in the rats with AMI exposed to the combined FGF21-KLB interventions, but not in the rats stimulated only with FGF21. Hence, the UTMD-mediated cardiac delivery of *KLB* helps restore FGF21 signaling, mitigating the impact of oxidative stress and mitochondrial dysfunction in myocardium post-MI. In agreement with previous research, targeting mitochondrial homeostasis is a potential therapeutic approach with which to attenuate adverse myocardial remodeling (3).

The Nrf2 protein is a primary transcription factor controlling the expression of various genes encoding antioxidant factors, detoxifying enzymes, drug transporters and other cytoprotective proteins (37). It potentially enhances the antioxidant signals against accumulative oxidative stress and regulates various aspects of energy metabolism and mitochondrial function (38). Specifically, Nrf2 enhances mitochondrial metabolism and the efficiency of ATP production by improving oxidative phosphorylation (38). In the present study, the combined FGF21-KLB interventions promoted the balance between oxidant and antioxidant signals by upregulating Nrf2 expression and downstream signals. When Nrf2 was inhibited, the protective effects of FGF21 administration and *KLB* delivery on cardiac function following infarction were significantly attenuated. Thus, these findings provide new insight into the role and mechanisms of the FGF21-KLB pathway in the heart post-infarction. The cardiac-targeted delivery of *KLB* assists FGF21 administration, significantly elevating antioxidant signals and inhibiting mitochondrial injury, which may be a potential strategy with which to prevent HF following AMI (8).

UTMD is an emerging technique for target-specific gene delivery with possible clinical utility (15). Compared to traditional MBs, CMBs exhibit a strong affinity for negatively charged plasmids, significantly enhancing the efficiency of gene delivery (10). The energy of low-frequency ultrasonic-mediated blasting is unlikely to cause cell oxidative injury (10). The present study combined the favorable features of different interdisciplinary patterns to effectively and safely carry genes to the heart. The findings presented herein confirm that the UTMD-mediated *KLB* delivery to the heart is a promising translational approach to optimize the effect of FGF21 administration. Consistent with previous research (8), the cardiac expression of *KLB* was significantly increased by target the blasting of CMBs, indicating that targeted gene delivery with CMBs and UTMD has promising prospects for clinical translation (13). Indeed, UTMD-mediated gene delivery is validated in translational studies involving islet regeneration in primates (39). Although other studies have found increased levels of circulating FGF21 following MI (9), the cardiac benefit of additional FGF21 supplementation is limited, raising concerns regarding the clinical translation of FGF21 therapy. The findings presented herein offer a feasible approach for addressing the undesirable effects of FGF21 therapy through UTMD-mediated receptor delivery. The combined *KLB*@CMB and FGF21 interventions effectively atteniated myocardial oxidative stress and mitochondrial damage induced post-infarction, significantly improving cardiac dysfunction and adverse remodeling.

In conclusion, the findings of the present study demonstrate that KLB co-receptor expression is significantly reduced in the myocardium following AMI, explaining the negligible effect of FGF21 in cardiometabolic disorders. A UTMD delivery system with CMBs carrying the *KLB* gene to the heart assists FGF21 treatment against cardiac adverse remodeling following AMI. As the targeted *KLB* delivery promotes the protective effect of FGF21 administration on the heart post-infarction, these results may provide distinctive perspectives on the translation of FGF21 administration into clinical; practice. Considering the excellent efficiency and biosafety of the UTMD system, the synergistic effect of FGF21 and *KLB*@CMBs appears to be a promising interdisciplinary approach for the prevention of heart dysfunction following AMI.

Acknowledgements

Not applicable.

Funding

The present study was supported by the Special Foundation for Basic Research Program of Yunnan Province Science and Technology Department and Kunming Medical University (grant no. 202201AY070001-217) and the Innovation Project of Qujing First People's Hospital (grant no. 2022YJKTY05).

Availability of data and materials

The datasets used and/or analyzed during the current study are available from the corresponding author on reasonable request.

Authors' contributions

CY, RLi and MY substantially contributed to the experimental conception and design of the study. CL, DZ and SL contributed to the acquisition of clinical data. CY, YY and TY contributed to the acquisition of data and analysis from *in vitro* experiments. CY, RLi, XH, YL, RLe, QY and QL contributed to the animal experiment. RLi and CL contributed to statistical analysis and visualization. CY and RLi were responsible for manuscript writing. All authors have read and approved the

final manuscript. MY supervised all experiments. All authors took the responsibility for the integrity and accuracy. CY and RLi confirm the authenticity of all the raw data.

Ethics approval and consent to participate

The clinical study protocols were approved by the Ethics Review Board of Qujing First People's Hospital, Qujing, China (approval no. QJFH2021-017). Written informed consent was obtained from all participants prior to enrollment. Ethical approval for the animal experiments was obtained from the Ethical Committee of Second Hospital of Kunming Medical University (approval no. kmmu 20211022 and kmmu 20221592). All animal experiments conducted in the present study followed the guidelines and regulations specified in this ethical approval.

Patient consent for publication

Not applicable.

Competing interests

The authors declare that they have no competing interests.

References

1. Ramachandra C, Hernandez-Resendiz S, Crespo-Avilan GE, Lin YH and Hausenloy DJ: Mitochondria in acute myocardial infarction and cardioprotection. EBioMedicine 57: 102884, 2020.
2. Wang S, Duan Y, Feng X, Liu L, Shi Z, Wang B, Xia C, Man W, Wang H, Zhao Z and Sun D: Sustained nicorandil administration reduces the infarct size in ST-segment elevation myocardial infarction patients with primary percutaneous coronary intervention. Anatol J Cardiol 21: 163-171, 2019.
3. Wang S, Zhao Z, Fan Y, Zhang M, Feng X, Lin J, Hu J, Cheng Z, Sun C, Liu T, *et al*: Mst1 inhibits Sirt3 expression and contributes to diabetic cardiomyopathy through inhibiting Parkin-dependent mitophagy. Biochim Biophys Acta Mol Basis Dis 1865: 1905-1914, 2019.
4. Chen S, Guan S, Yan Z, Ouyang F, Li S, Liu L and Zhong J: Role of RIPK3-CaMKII-mPTP signaling pathway-mediated necroptosis in cardiovascular diseases (review). Int J Mol Med 52: 98, 2023.
5. Jin L, Geng L, Ying L, Shu L, Ye K, Yang R, Liu Y, Wang Y, Cai Y, Jiang X, *et al*: FGF21-sirtuin 3 axis confers the protective effects of exercise against diabetic cardiomyopathy by governing mitochondrial integrity. Circulation 146: 1537-1557, 2022.
6. Tao Z, Cui Y, Xu X and Han T: FGFR redundancy limits the efficacy of FGFR4-selective inhibitors in hepatocellular carcinoma. Proc Natl Acad Sci USA 119: e2208844119, 2022.
7. Romanello V: The interplay between mitochondrial morphology and myomitokines in aging sarcopenia. Int J Mol Sci 22: 91, 2020.
8. Jimenez V, Jambrina C, Casana E, Sacristan V, Munoz S, Darriba S, Rodó J, Mallol C, Garcia M, León X, *et al*: FGF21 gene therapy as treatment for obesity and insulin resistance. EMBO Mol Med 10: e8791, 2018.
9. Zhang W, Chu S, Ding W and Wang F: Serum level of fibroblast growth factor 21 is independently associated with acute myocardial infarction. PLoS One 10: e0129791, 2015.
10. Wang S, Chen K, Wang Y, Wang Z, Li Z, Guo J, Chen J, Liu W, Guo X, Yan G, *et al*: Cardiac-targeted delivery of nuclear receptor RORα via ultrasound targeted microbubble destruction optimizes the benefits of regular dose of melatonin on sepsis-induced cardiomyopathy. Biomater Res 27: 41, 2023.
11. Li H, Zhang Y, Shu H, Lv W, Su C and Nie F: Highlights in ultrasound-targeted microbubble destruction-mediated gene/drug delivery strategy for treatment of malignancies. Int J Pharm 613: 121412, 2022.
12. Zheng J, Huang J, Zhang L, Wang M, Xu L, Dou X, Leng X, Fang M, Sun Y and Wang Z: Drug-loaded microbubble delivery system to enhance PD-L1 blockade immunotherapy with remodeling immune microenvironment. Biomater Res 27: 9, 2023.
13. Omata D, Unga J, Suzuki R and Maruyama K: Lipid-based microbubbles and ultrasound for therapeutic application. Adv Drug Deliv Rev 154-155: 236-244, 2020.
14. Beccaria K, Sabbagh A, de Groot J, Canney M, Carpentier A and Heimberger AB: Blood-brain barrier opening with low intensity pulsed ultrasound for immune modulation and immune therapeutic delivery to CNS tumors. J Neurooncol 151: 65-73, 2021.
15. Carpentier A, Canney M, Vignot A, Reina V, Beccaria K, Horodyckid C, Karachi C, Leclercq D, Lafon C, Chapelon JY, *et al*: Clinical trial of blood-brain barrier disruption by pulsed ultrasound. Sci Transl Med 8: 343re2, 2016.
16. Chen K, Bai L, Lu J, Chen W, Liu C, Guo E, Qin X, Jiao X, Huang M and Tian H: Human decidual mesenchymal stem cells obtained from early pregnancy improve cardiac revascularization postinfarction by activating ornithine metabolism. Front Cardiovasc Med 9: 837780, 2022.
17. Liu Y, Zhou J, Luo Y, Li J, Shang L, Zhou F and Yang S: Honokiol alleviates LPS-induced acute lung injury by inhibiting NLRP3 inflammasome-mediated pyroptosis via Nrf2 activation in vitro and in vivo. Chin Med 16: 127, 2021.
18. Hu Z, Ju F, Du L and Abbott GW: Empagliflozin protects the heart against ischemia/reperfusion-induced sudden cardiac death. Cardiovasc Diabetol 20: 199, 2021.
19. Safari F, Hajizadeh S, Shekarforoush S, Bayat G, Foadoddini M and Khoshbaten A: Influence of ramiprilat and losartan on ischemia reperfusion injury in rat hearts. J Renin Angiotensin Aldosterone Syst 13: 29-35, 2012.
20. Tang MN, Hu JL and Yan Y: The efficacy and mechanism of renal denervation (RD) versus drugs in treating post-acute myocardial infarction (AMI) heart failure (HF) in rats. Fudan Univ J Med Sci 46: 584-591, 2019.
21. Xu J, Lloyd DJ, Hale C, Stanislaus S, Chen M, Sivits G, Vonderfecht S, Hecht R, Li YS, Lindberg RA, *et al*: Fibroblast growth factor 21 reverses hepatic steatosis, increases energy expenditure, and improves insulin sensitivity in diet-induced obese mice. Diabetes 58: 250-259, 2009.
22. Du GQ, Shao ZB, Wu J, Yin WJ, Li SH, Wu J, Weisel RD, Tian JW and Li RK: Targeted myocardial delivery of GDF11 gene rejuvenates the aged mouse heart and enhances myocardial regeneration after ischemia-reperfusion injury. Basic Res Cardiol 112: 7, 2017.
23. Muskula PR and Main ML: Safety with echocardiographic contrast agents. Circ Cardiovasc Imaging 10: e005459, 2017.
24. Borrelli MJ, O'Brien WJ Jr, Hamilton E, Oelze ML, Wu J, Bernock LJ, Tung S, Rokadia H and Culp WC: Influences of microbubble diameter and ultrasonic parameters on in vitro sonothrombolysis efficacy. J Vasc Interv Radiol 23: 1677-1684. e1, 2012.
25. Wang Z, Jiang S, Li S, Yu W, Chen J, Yu D, Zhao C, Li Y, Kang K, Wang R, *et al*: Targeted galectin-7 inhibition with ultrasound microbubble targeted gene therapy as a sole therapy to prevent acute rejection following heart transplantation in a rodent model. Biomaterials 263: 120366, 2020.
26. Wang S, Zhao Z, Feng X, Cheng Z, Xiong Z, Wang T, Lin J, Zhang M, Hu J, Fan Y, *et al*: Melatonin activates Parkin translocation and rescues the impaired mitophagy activity of diabetic cardiomyopathy through Mst1 inhibition. J Cell Mol Med 22: 5132-5144, 2018.
27. Fang X, Wang H, Han D, Xie E, Yang X, Wei J, Gu S, Gao F, Zhu N, Yin X, *et al*: Ferroptosis as a target for protection against cardiomyopathy. Proc Natl Acad Sci USA 116: 2672-2680, 2019.
28. Aishwarya R, Alam S, Abdullah CS, Morshed M, Nitu SS, Panchatcharam M, Miriyala S, Kevil CG and Bhuiyan MS: Pleiotropic effects of mdivi-1 in altering mitochondrial dynamics, respiration, and autophagy in cardiomyocytes. Redox Biol 36: 101660, 2020.
29. Livak KJ and Schmittgen TD: Analysis of relative gene expression data using real-time quantitative PCR and the 2(-Delta Delta C(T)) method. Methods 25: 402-408, 2001.
30. Wang S, Fan Y, Feng X, Sun C, Shi Z, Li T, Lv J, Yang Z, Zhao Z and Sun D: Nicorandil alleviates myocardial injury and post-infarction cardiac remodeling by inhibiting Mst1. Biochem Biophys Res Commun 495: 292-299, 2018.
31. Burtscher J, Soltany A, Visavadiya NP, Burtscher M, Millet GP, Khoramipour K and Khamoui AV: Mitochondrial stress and mitokines in aging. Aging Cell 22: e13770, 2023.

32. Yang M, Liu C, Jiang N, Liu Y, Luo S, Li C, Zhao H, Han Y, Chen W, Li L, *et al*: Fibroblast growth factor 21 in metabolic syndrome. Front Endocrinol (Lausanne) 14: 1220426, 2023.
33. Tsutsui H, Albert NM, Coats A, Anker SD, Bayes-Genis A, Butler J, Chioncel O, Defilippi CR, Drazner MH, Felker GM, *et al*: Natriuretic peptides: Role in the diagnosis and management of heart failure: A scientific statement from the heart failure association of the European society of cardiology, heart failure society of America and Japanese heart failure society. Eur J Heart Fail 25: 616-631, 2023.
34. Wei YJ, Wang JF, Cheng F, Xu HJ, Chen JJ, Xiong J and Wang J: miR-124-3p targeted SIRT1 to regulate cell apoptosis, inflammatory response, and oxidative stress in acute myocardial infarction in rats via modulation of the FGF21/CREB/PGC1α pathway. J Physiol Biochem 77: 577-587, 2021.
35. Bäck M, Caldenius V, Svensson L and Lundberg M: Perceptions of kinesiophobia in relation to physical activity and exercise after myocardial infarction: A qualitative study. Phys Ther 100: 2110-2119, 2020.
36. Wang S, Liu Y, Liu J, Tian W, Zhang X, Cai H, Fang S and Yu B: Mitochondria-derived methylmalonic acid, a surrogate biomarker of mitochondrial dysfunction and oxidative stress, predicts all-cause and cardiovascular mortality in the general population. Redox Biol 37: 101741, 2020.
37. Silva-Palacios A, Ostolga-Chavarria M, Zazueta C and Königsberg M: Nrf2: Molecular and epigenetic regulation during aging. Ageing Res Rev 47: 31-40, 2018.
38. Esteras N and Abramov AY: Nrf2 as a regulator of mitochondrial function: Energy metabolism and beyond. Free Radic Biol Med 189: 136-153, 2022.
39. Zhang C, Chen S, Li Q, Wu J, Qiu F, Chen Z, Sun Y, Luo J, Bastarrachea RA, Grayburn PA, *et al*: Ultrasound-targeted microbubble destruction mediates gene transfection for beta-cell regeneration and glucose regulation. Small 17: e2008177, 2021.